Inverter Based Resource Power Oscillations Damping Control

Technical Brief — *Transmission Operations & Bulk System Renewables and Distributed Energy Resources Integration*

Introduction

In today's interconnected power grids, low-frequency oscillations is a significant issue that can limit the power transfer capability and even deteriorate power system security due to potential low-damped or even undamped oscillations. The increasing integration of renewable energy sources may create more severe, complex, and frequent oscillations. If not sufficiently controlled, these oscillations can lead to major blackout events that cost billions of dollars. Effective suppression of various oscillations is essential to maintain the secure and reliable operation of power grids.

Typically, local controllers (e.g., power system stabilizers on generators) have been used to suppress these low-frequency oscillations. However, the retirement of conventional plants will result in insufficient stabilizing capability from the remaining generators, the location of which may also render them inappropriate to suppress these oscillations. Use of inverter-based resources (IBRs) with appropriate controls to provide damping is envisioned as a solution to this challenge. Due to the power electronics interface with the grid, these devices can provide fast and flexible control that can outperform slower control provided by generators.

This work investigated the potential of using IBRs as actuators of power oscillation damping (POD) control to suppress low-frequency oscillations. A synthetic Texas power grid model was used as the study system. The optimal observation signals were selected among local signals and remote signals. The control performance is validated and compared when using local signal and remote signals as the input of the controller. Also, the control performance of local POD and wide-area POD is compared under active power modulation and reactive power modulation.

This report is organized as follows: The modal analysis of the synthetic Texas power grid model is introduced in Chapter 2. Chapter 3 presents the optimal observation signal selection and the optimal actuator selection for both wide-area POD and local POD on IBRs. The performance of the wide-area POD and local POD is validated and compared in Chapter 4. A summary and future work are given in Chapter 5, followed by references in Chapter 6.

Modal Analysis of Synthetic Texas Power Grid Model

In this chapter, modal analysis was conducted on the 2000-bus synthetic Texas power grid model. Two dominant oscillation modes were identified by using model based small-signal analysis and Prony analysis of dynamic simulation results. The properties of the two oscillation modes were obtained, including oscillation frequency, damping ratio, and mode shape.

Model Description

The 2000-bus synthetic Texas power grid model was used in this work. The model has been built from publicly available information by Texas A&M University [1]. As shown in Figure 1, the system has 8 areas, of which Area 5 is the load center. The red arrows indicate the power flow directions among these areas. There is a large power transfer from Area 7 (Coast) and Area 8 (East) to Area 5 (North Central).

Figure 1. Area map of synthetic Texas power grid model.

Addition of Renewable Dynamic Models

The main objective of this work is to compare the control performance of local POD and wide-area POD via IBRs. Since the original synthetic Texas power grid model has no dynamic models for IBRs, IBR dynamic models have been added to the network model. To facilitate the optimal actuator selection, at least one renewable generator in each zone of each area is considered. The IBRs are modeled using dynamic models developed under the Western Electricity Coordinating Council (WECC) Renewable Energy Modeling Task Force [2]. In particular, the IBRs are modeled using the following two modules: generator/converter model

(REGCAU2), and electrical control model (REECCU1). Typical parameters were used in this work.

Table 1. IBRs added in synthetic Texas power grid model

Area & Zone	IBR bus	Capacity (MW)
Area 6 Zone 22	6069	500
Area 6 Zone 23	6214	500
Area 6 Zone 24	6266	500
Area 6 Zone 25	6006	500
Area 6 Zone 26	6051	500
Area 7 Zone 1	7098	500
Area 7 Zone 2	7422	500
Area 7 Zone 3	7179	500
Area 7 Zone 4	7005	500
Area 7 Zone 5	7389	500
Area 7 Zone 6	7406	500
Area 8 Zone 7	8046	500
Area 8 Zone 8	8077	500

Small-Signal Analysis and Dynamic Simulations

Small-signal analysis was conducted on the modified model in DSAtools/SSAT to understand the dominant oscillation modes. The small-signal analysis results are given in Figure 2 and Table 2. There are two dominant oscillation modes in this model. One is between Area 4 and Area 7, whose oscillation frequency is 0.67 Hz, and the damping ratio is 5.10%. The other is between Area 1, 2, 3, 4, 5, west Area 8 and Area 7, east Area 8, whose oscillation frequency is 0.60 Hz, and the damping ratio is 6.31%.

These two dominant oscillation modes were also verified by time-domain simulations. For a temporary three-phase fault applied at the line between Bus 4040 and Bus 4079, the bus frequency signals in Area 4 are oscillating against those in Area 7, as shown in Figure 3 (a). Similarly, for a temporary three-phase fault applied to the line between Bus 8030 and Bus 8158, the oscillation Mode 2 can be observed in Figure 3 (b). As given in Table 3, Prony analysis [3] of the bus frequency signals shows that the oscillation frequency and damping ratio obtained from Prony analysis are close to those results from model-based small-signal analysis.

Table 2. Small-signal analysis results in SSAT

	Frequency (Hz)	Damping ratio (%)
Mode 1	0.67	5.10
Mode 2	0.60	6.31

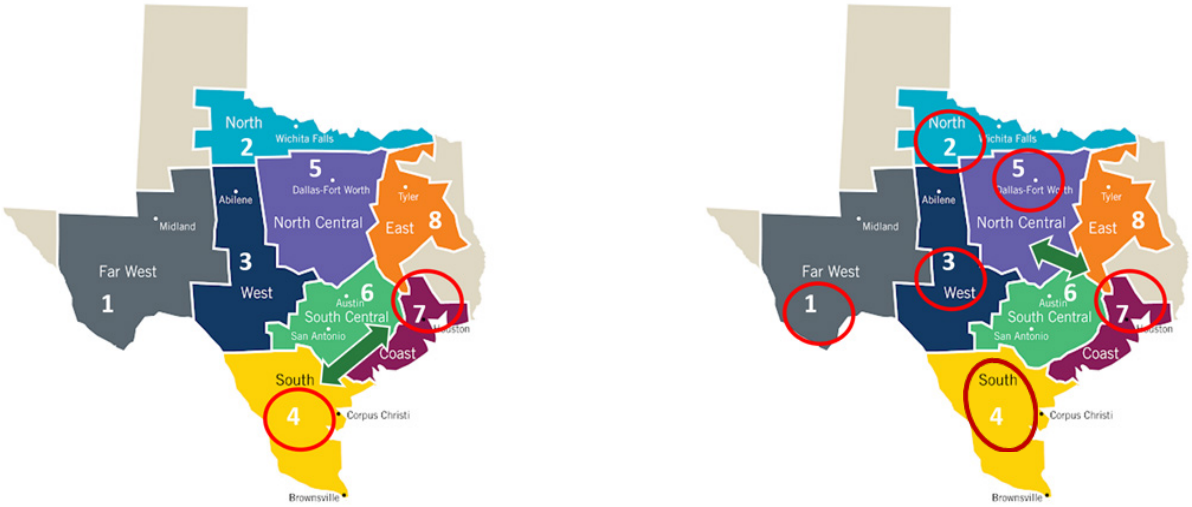

(a) Mode 1 **(b) Mode 2**

Figure 2. Mode shape of two modes

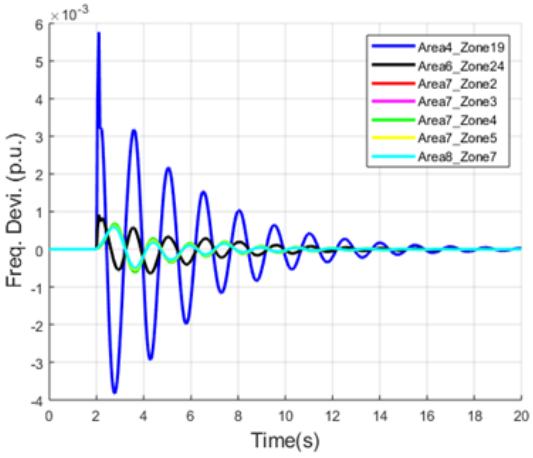

(a) Mode 1

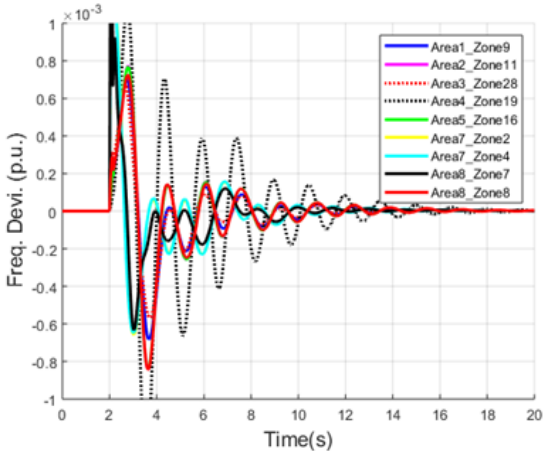

(b) Mode 2

Figure 3. Bus frequency under three-phase temporary fault.

Table 3. Prony analysis results in PSS/E dynamic simulation

	Frequency (Hz)	Damping ratio (%)
Mode 1	0.67	6.22
Mode 2	0.63	8.70

Optimal Observation Signal and Actuator Selection of POD Control

In this chapter, the optimal wide-area observation signal was selected for wide-area POD through IBR and synchronous generators. The selection of the optimal observation signal indicates the desired location of PMUs that will provide the input signal to the wide-area POD. Local IBR PODs will adopt the local bus frequency as the POD input signal. After selecting the optimal observation signals, the optimal actuator was chosen among renewables and synchronous generators in the synthetic Texas power system. Fast Fourier transform (FFT) analysis was used to select the optimal observation signal, while the residue method was utilized to select the optimal actuation signal [4-8].

Optimal Observation Signal and Actuator Selection for Wide-area POD Control

Optimal Observation Signal Selection for Wide-Area POD Control

The synthetic Texas power system includes a great number of candidate observation signals for oscillation mode analysis. However, since only some of them have good observability of both Mode 1 and Mode 2, in this work, FFT was adopted to select the optimal observation signals of the damping control loop by extracting the measurement signals to the frequency domain.

Fourier analysis converts sampling rate (or space) to frequency or vice versa. The FFT algorithm can rapidly compute such transformations by factorizing the discrete Fourier transform matrix into a product of sparse (mostly zero) factors. The function *Y=fft(x)* is given for vectors of length *N* by:

$$X(k) = \sum_{j=0}^{N-1} x(j)\omega_N^{jk} \qquad 0 \le k \le N-1$$

where

$$\omega_N = e^{(-2\pi i)/N}$$

is an N-*th* root of unity.

Different three-phase fault events at different locations were used to excite both modes. For each case, the normalized FFT results of each measurement signal at the oscillation frequencies of the two modes are shown in Table 4 and Table 5. Based on the mode shape analysis, the green cells indicate one coherent group of generators, while the yellow ones indicate the other coherent group, in the opposite direction of the first one. The coherent oscillation groups of the two modes are shown in Figure 4 (a) and (b). To guarantee the best damping performance of both modes, the measurement signals with the largest magnitudes and the same oscillation shape are selected. The frequency difference between the two opposite oscillation sides is selected as the optimal observation signal for suppressing the two modes.

Table 4. FFT results of optimal wide-area observation signal selection under event in Zone 4

Bus	Area & Zone	Mode 1 (0.67Hz, 6.1%)	Mode 2 (0.63Hz, 8.5%)
1004	Area 1 Zone 9	0.09	0.08
1079	Area 1 Zone 9	0.10	0.08
2002	Area 2 Zone 11	0.14	0.11
2017	Area 2 Zone 10	0.11	0.09
3048	Area 3 Zone 27	0.10	0.08
3036	Area 3 Zone 28	0.05	0.06
4192	**Area 4 Zone 19**	**1.00**	**0.89**
4195	Area 4 Zone 20	0.37	0.34
4181	Area 4 Zone 21	0.66	0.73
5018	Area 5 Zone 12	0.12	0.10
5137	Area 5 Zone 13	0.10	0.08
5179	Area 5 Zone 14	0.12	0.09
5120	Area 5 Zone 15	0.09	0.08
5049	Area 5 Zone 16	0.14	0.11
5015	Area 5 Zone 17	0.14	0.11
5317	Area 5 Zone 18	0.13	0.10
6056	Area 6 Zone 22	0.09	0.10
6021	Area 6 Zone 23	0.04	0.06
6263	Area 6 Zone 24	0.18	0.17
6107	Area 6 Zone 25	0.04	0.05
6045	Area 6 Zone 26	0.09	0.10
7095	Area 7 Zone 1	0.03	0.03
7320	Area 7 Zone 2	0.12	0.12
7037	Area 7 Zone 3	0.10	0.11
7076	**Area 7 Zone 4**	**0.12**	**0.12**
7175	Area 7 Zone 5	0.10	0.11
7042	Area 7 Zone 6	0.08	0.08
8030	Area 8 Zone 7	0.09	0.09
8074	Area 8 Zone 8	0.15	0.12

Table 5. FFT results of optimal wide-area observation signal selection under event in Zone 8

Bus	Area & Zone	Mode 1 (0.67Hz, 6.1%)	Mode 2 (0.63Hz, 8.5%)
1004	Area 1 Zone 9	0.23	0.37
1079	Area 1 Zone 9	0.24	0.38
2002	Area 2 Zone 11	0.28	0.48
2017	Area 2 Zone 10	0.25	0.41
3048	Area 3 Zone 27	0.24	0.39
3036	Area 3 Zone 28	0.21	0.31
4192	**Area 4 Zone 19**	**0.89**	**1.00**
4195	Area 4 Zone 20	0.40	0.46
4181	Area 4 Zone 21	0.67	0.75
5018	Area 5 Zone 12	0.27	0.44
5137	Area 5 Zone 13	0.24	0.39
5179	Area 5 Zone 14	0.26	0.42
5120	Area 5 Zone 15	0.24	0.38
5049	Area 5 Zone 16	0.28	0.47
5015	Area 5 Zone 17	0.28	0.46
5317	Area 5 Zone 18	0.27	0.44
6056	Area 6 Zone 22	0.20	0.25
6021	Area 6 Zone 23	0.20	0.28
6263	Area 6 Zone 24	0.23	0.27
6107	Area 6 Zone 25	0.19	0.29
6045	Area 6 Zone 26	0.21	0.26
7095	Area 7 Zone 1	0.09	0.08
7320	Area 7 Zone 2	0.21	0.23
7037	Area 7 Zone 3	0.18	0.19
7076	**Area 7 Zone 4**	**0.22**	**0.23**
7175	Area 7 Zone 5	0.18	0.19
7042	Area 7 Zone 6	0.13	0.15
8030	Area 8 Zone 7	0.14	0.13
8074	Area 8 Zone 8	0.27	0.47

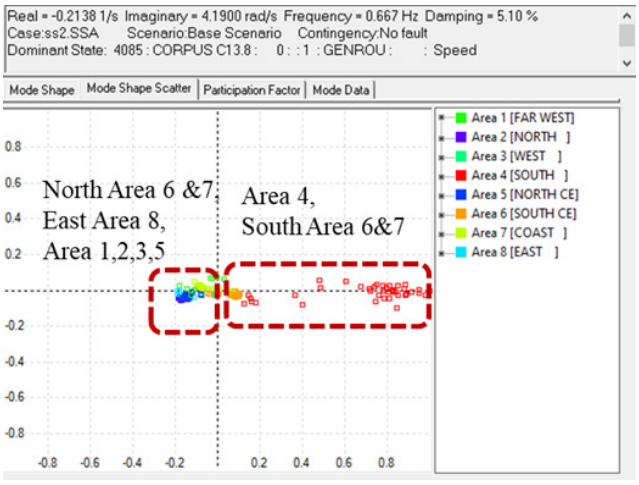

(a) Mode 1

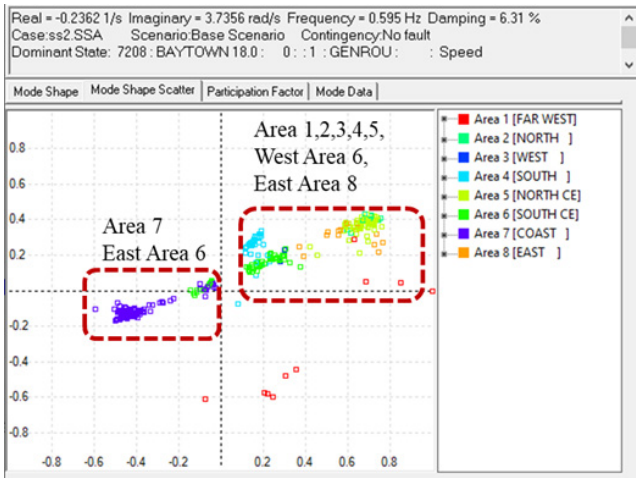

(b) Mode 2

Figure 4. Coherent oscillation group of the two different modes.

As shown in the above two tables and coherent oscillation group figure, bus frequency 4192 in Area 4 Zone 19 has the maximum FFT magnitude for Mode 1 and Mode 2 on the same oscillation side, while bus frequency 7076 in Area 7 Zone 4 has the maximum FFT magnitude for Mode 1 and Mode 2 on the opposite oscillation side. The frequency difference between bus 4192 and 7076 is selected as the optimal observation signal for wide-area PODs.

Optimal IBR Actuator Selection for Wide-Area POD Control

Different IBRs and synchronous generators have different controllability to the system oscillation modes. A method to analyze the sensitivity of all candidate actuators to the observation signal was developed to select the optimal actuation signals.

The transfer function $g_{[ij]}(s)$ is obtained from the input u_i to the output y_j, and it can always be expressed as a sum of partial fractions of the form

$$g_{ij}(s) = \sum_{k=1}^{n} \frac{R_k}{s-\lambda_k}$$

where R_k is the residue associated with the mode λ_k. The residue R_k provides an idea of how the mode λ_k is affected by the input u_i and how visible it is from the output y_j. Therefore, the residues are clear measures of joint controllability and observability of a particular oscillation mode. For this reason, residues are commonly used in damping oscillation analysis.

For most of the state-of-the-art research, the residues are computed directly from the state-space realization by using

$$R_k = c\emptyset_k\varphi_k b$$

where $\emptyset_k$ and φ_k are the right and left eigenvectors of the state matrix A, respectively, corresponding to the eigenvalue λ_k, c is the output vector and b is input vector of the state space model.

Generally, the residues are complex numbers, and the optimal input-output signal pair is given by the maximum value of the residue magnitude. Since the wide-area observation signals have been selected, the controllability of each actuator can be reflected by the residue magnitude. The IBRs or synchronous generators with the largest residues will be selected as the wide-area POD actuators.

The residue of IBR actuator is calculated between its active power/reactive power reference and the wide-area feedback signal. Table 6 lists the normalized residue magnitude and phase angle of Mode 1 and Mode 2 for each candidate IBR actuator through active power modulation. As shown in the table, IBR 4153 with the highest magnitude at Mode 1 will be selected to control Mode 1. IBR 7422 with the highest magnitude at Mode 2 will be selected to control Mode 2.

Table 6. Residue identification results of optimal IBR actuators for wide-area POD

IBR Bus	Area & Zone	Mode 1		Mode 2	
		Mag.	Angle (°)	Mag.	Angle (°)
1004	Area 1 Zone 9	0.2245	-176	0.2449	7
2127	Area 2 Zone 10	0.5102	-137	0.2245	50
2071	Area 2 Zone 11	0.2653	165	0.2245	-10
3081	Area 3 Zone 27	0.2244	-147	0.2445	40
3074	Area 3 Zone 28	N/A	N/A	0.0816	-28
4183	Area 4 Zone 19	0.7347	-7	N/A	N/A
4177	Area 4 Zone 20	0.3266	-8	N/A	N/A
4153	**Area 4 Zone 21**	**1**	**-5**	N/A	N/A
5238	Area 5 Zone 12	0.2857	-178	0.2857	4
5399	Area 5 Zone 15	0.2041	-158	0.2041	24
5243	Area 5 Zone 18	0.0816	162	0.0816	-11
6069	Area 6 Zone 22	N/A	N/A	0.1224	-4
6214	Area 6 Zone 23	0.1837	-94	0.2041	66
6006	Area 6 Zone 25	0.1224	-54	N/A	N/A
7098	Area 7 Zone 1	N/A	N/A	0.1224	134
7422	**Area 7 Zone 2**	N/A	N/A	**0.3265**	**168**
7170	Area 7 Zone 3	N/A	N/A	0.2857	170
7005	Area 7 Zone 4	0.3878	164	N/A	N/A
7389	Area 7 Zone 5	0.4082	149	N/A	N/A
8077	Area 8 Zone 8	0.4082	-153	0.3673	39

Optimal Synchronous Generator Actuator Selection for Wide-Area POD Control

The residue of each synchronous generator actuator is calculated between its voltage reference and the wide-area feedback signal. Table 7 lists the normalized residue magnitude and phase angle of Mode 1 and Mode 2 for each candidate synchronous generator actuator. As shown in the table, generator 4030 with the highest magnitude at Mode 1 will be selected to control Mode 1. Generator 7208 with the highest magnitude at Mode 2 will be selected to control Mode 2.

Table 7. Residue identification results of optimal synchronous generator actuators for wide-area POD

Gen. Bus	Area & Zone	Mode 1(0.67Hz)		Mode 2 (0.63Hz)	
		Mag	Ang(°)	Mag	Ang(°)
1072	Area 1 Zone 9	N/A	N/A	0.0702	-88
2075	Area 2 Zone 11	0.2105	-112	0.2281	73
3106	Area 3 Zone 28	N/A	N/A	N/A	N/A
4192	Area 4 Zone 19	0.2982	84	N/A	N/A
4026	Area 4 Zone 20	0.1930	100	N/A	N/A
4030	**Area 4 Zone 21**	**0.4386**	**126**	N/A	N/A
5058	Area 5 Zone 12	0.2105	-70	0.2281	110
5360	Area 5 Zone 13	0.8947	14	1	-158
5382	Area 5 Zone 14	N/A	N/A	N/A	N/A
5302	Area 5 Zone 16	0.2281	-30	0.2631	155
5067	Area 5 Zone 17	0.2807	-80	0.2807	101
5262	Area 5 Zone 18	0.1228	-132	0.1228	54
6145	Area 6 Zone 22	0.1228	90	N/A	N/A
6214	Area 6 Zone 23	0.0351	-152	0.0175	49
6274	Area 6 Zone 24	N/A	N/A	N/A	N/A
6078	Area 6 Zone 25	N/A	N/A	0.0175	-126
6051	Area 6 Zone 26	N/A	N/A	0.0175	105
7099	Area 7 Zone 1	N/A	N/A	0.0351	-175
7422	Area 7 Zone 2	N/A	N/A	N/A	N/A
7353	Area 7 Zone 3	N/A	N/A	0.0175	-115
7208	**Area 7 Zone 4**	0.1667	164	**0.2807**	**-100**
7389	Area 7 Zone 5	0.1754	149	0.2631	-99
7406	Area 7 Zone 6	N/A	N/A	N/A	N/A
8071	Area 8 Zone 7	0.1053	-27	0.1228	154
8129	Area 8 Zone 8	0.1579	-130	0.1579	58

Optimal Actuator Selection for Local IBR POD Control

Different from wide-area PODs, local PODs will adopt the local bus frequency difference as its feedback signal. Table 8 lists the normalized residue magnitude and phase angle of Mode 1 and Mode 2 for each candidate local IBR actuator. As shown in the table, IBR 4153 with the highest magnitude at Mode 1 will be selected to control Mode 1. IBR 8077 with the highest magnitude at Mode 2 will be selected to control Mode 2.

Table 8. Residue identification results of optimal IBR actuators for local POD

Bus	Zone Area	Mode 1		Mode 2	
		Mag.	Angle (°)	Mag.	Angle (°)
1004	Area 1 Zone 9	0.2778	170	0.2778	7
2127	Area 2 Zone 10	0.3333	-170	0.3889	17
2071	Area 2 Zone 11	N/A	N/A	0.1667	30
3081	Area 3 Zone 27	N/A	N/A	0.3333	-15
3074	Area 3 Zone 28	N/A	N/A	N/A	N/A
4183	Area 4 Zone 19	0.7778	-8	N/A	N/A
4177	Area 4 Zone 20	N/A	N/A	N/A	N/A
4153	Area 4 Zone 21	**1.0000**	**-6**	N/A	N/A
5238	Area 5 Zone 12	N/A	N/A	0.3333	4
5399	Area 5 Zone 15	0.1667	-166	0.2222	-5
5243	Area 5 Zone 18	0.1111	180	0.0556	10
6069	Area 6 Zone 22	N/A	N/A	0.0556	0
6214	Area 6 Zone 23	N/A	N/A	N/A	N/A
6006	Area 6 Zone 25	N/A	N/A	N/A	N/A
7098	Area 7 Zone 1	N/A	N/A	N/A	N/A
7422	Area 7 Zone 2	N/A	N/A	0.1111	-33
7170	Area 7 Zone 3	N/A	N/A	0.1111	-30
7005	Area 7 Zone 4	N/A	N/A	0.1667	-40
7389	Area 7 Zone 5	0.0556	-79	N/A	N/A
8077	Area 8 Zone 8	0.5000	39	**0.5000**	**0**

POD Control Design and Performance Assessment

POD Controller Structure

In this work, the POD controller is based on the lead-lag structure, which consists of a washout block, a filter, two phase compensation blocks, a gain block, and a rate limiter [9-13]. Figure 5 illustrates the block diagram of the POD controller. The input signal of POD is a selected wide-area frequency difference or local bus frequency. The rate limiter is set to be 1 p.u./s to avoid the rapid change of active/reactive power output.

The electrical model of IBR in this study consists of generator/converter model (REGCAU2) and electrical control model (REECCU1) in PSS/E. Active power modulation control command from POD is added as an auxiliary signal to Paux to the REECCU1 model to modulate the active current of the IBRs, as shown in Figure 5 (a). To guarantee the effectiveness of active power modulation, the IBRs are set to have 200MW output, below their nominal capacity. Reactive power modulation control command from POD is added to pfaref to modulate the power factor of the IBRs, as shown in Figure 6 (b). Variables PfFlag, VFlag, and QFlag are set to be 1.

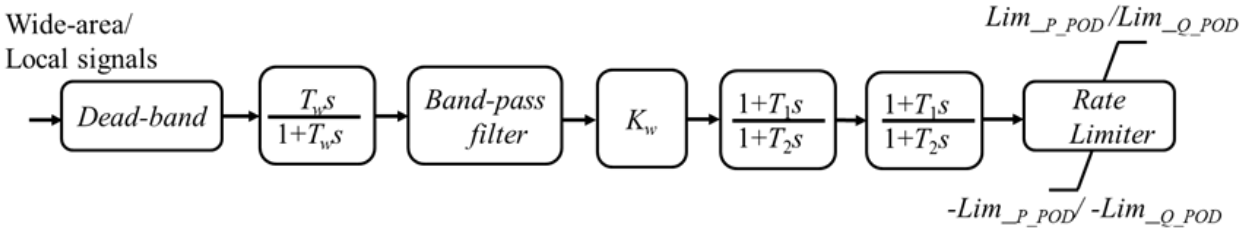

Figure 5. POD Structure

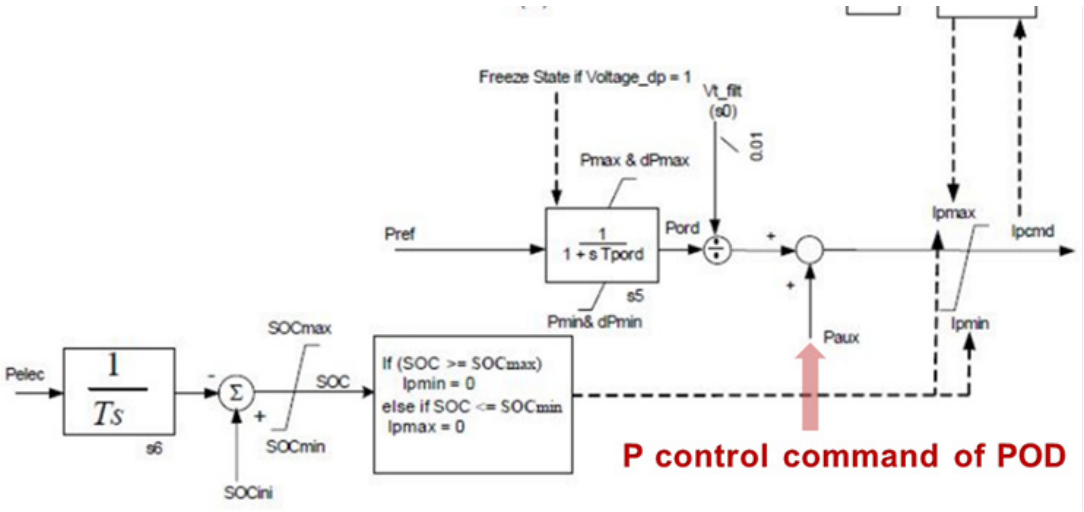

(a) Active power modulation of IBRs with POD

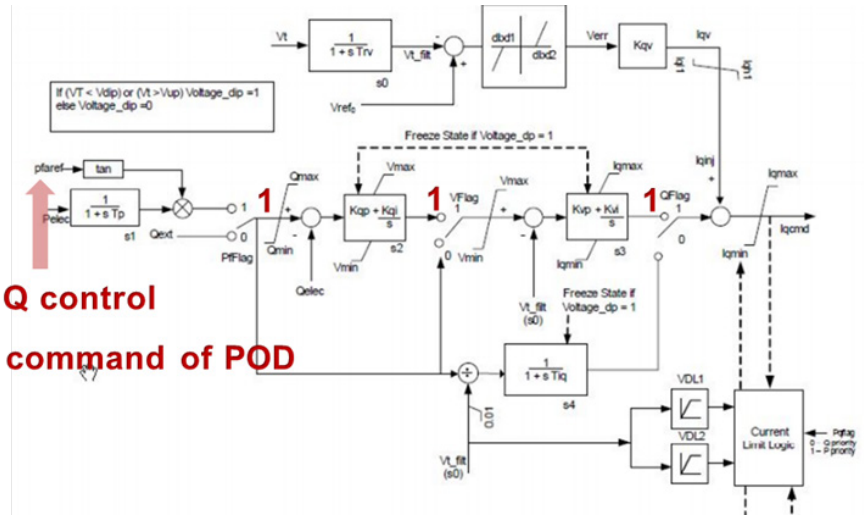

(b) Reactive power modulation of IBRs with POD

Figure 6. Diagram of active/reactive power modulation of IBRs with POD

POD Control Design Method

The time constant T_w of the washout block is 10s. The transfer function of the filter is [13]:

$$K_f(s) = \frac{\frac{\omega_n}{Q}s}{s^2+\frac{\omega_n}{Q}s+\omega_n^2}$$

where ω_n is the oscillation frequency of the targeted mode. Q is the quality factor, which is usually set to be 1.

The compensation phase and gain are the key parameters that determine the controller performance, and should be carefully designed. When modulating active/reactive power of IBRs, the compensation phase and gain can be calculated based on the transfer function of the power system model. The transfer function can always be transformed as a sum of partial fractions of the form

$$g_{ij}(s) = \sum_{k=1}^{n} \frac{R_k}{s-\lambda_k}$$

where R_k is the residue associated with the mode λ_k. The residue R_k provides an idea of how the mode λ_k is affected by the input u and how visible it is from the output y.

According to R_k associated with the inter-area oscillation mode λ_k, the compensation angle of POD should satisfy

$$\angle K(j\omega_d) + \angle R_k = -180°$$

and the amplitude should satisfy

$$|K(j\omega_d)| \cdot |R_k| = |-(\zeta_* - \zeta_k)\omega_d|$$

where ω_n and ζ_k are the frequency and damping ratio of the dominant inter-area oscillation mode. ζ_* is the expected damping ratio.

The parameters of *K*(s) can be calculated with the following equations:

POD was implemented in Python and integrated with PSS/E for the grid simulation.

$$\begin{cases} \alpha = \frac{1+sin\theta_{max}}{1-sin\theta_{max}}, \ \theta_{max} = \angle K(j\omega_n)/2 \\ T_1 = T_3 = \alpha T_2, \ T_2 = T_4 == \frac{1}{\sqrt{\alpha}\omega_{dn}} \\ K_w = \frac{|K(j\omega_{dn})|}{(\left|\frac{1+T_1 s}{1+T_2 s}\right|_{s=j\omega_{dn}})^2} \end{cases}$$

Wide-Area POD Control Design with Active/Reactive Power Modulation of IBR

Wide-Area POD Control Design with Active Power Modulation of IBR

Based on the optimal observation signal selection results in Chapter 3, the wide-area POD with active power modulation of IBR in the synthetic Texas power grid will adopt the bus frequency difference between Area 4 and Area 7 (*f4-f7*) as its feedback signal. The parameters of PODs are calculated according to the method introduced in *POD Control Design Method*. Table 9 lists the parameters of the wide-area POD controllers for modulating the active power of renewable generator 4153 and 7422. The active power modulation amplitude is usually limited within ±10% [14].

Wide-Area POD Control Design with Reactive Power Modulation of IBR

Similar to PODs for active power modulation of IBRs, the wide-area POD with reactive power modulation of IBR in the synthetic Texas power grid will adopt the same bus frequency difference signal between Area 4 and Area 7 (*f4-f7*) as its feedback signal.

Table 10 lists the parameters of the wide-area POD controllers for modulating the reactive power of renewable generator 4153 and 7422. According to Figure 6 (b), the reactive power modulation maximum amplitude is set to be $Lim_{\_Q\_WADC}$ = atan (Qmax/Pelec).

Local IBR POD Control Design with Active/Reactive Power Modulation

Local IBR POD Control Design with Active Power Modulation

Local POD in the synthetic Texas power grid will adopt the local bus frequency as its feedback signal. Table 11 lists the parameters of the local POD controllers for modulating the active power of renewable generator 4153 and 8077. The active power modulation amplitude is usually limited within ±10%.

Local IBR POD Control Design with Reactive Power Modulation

Similar to local POD for active power modulation of IBRs, the local POD with reactive power modulation of IBR in the synthetic Texas power grid will adopt the same local bus frequency as its feedback signal.

Table 12 lists the parameters of the local POD controllers for modulating the reactive power of renewable generator 4153 and 8077.

Table 9. Parameters of wide-area PODs with active power modulation

POD location	Tw (washout)	Wn (filter)	K (control gain)	T1 (phase shift)	T2 (phase shift)	$Lim_{\_P\_POD}$ (limiter)
4153	10	4.21	145	0.2375	0.2375	0.1
7422	10	3.96	-281	0.2806	0.2275	0.1

Table 10. Parameters of wide-area PODs with reactive power modulation

POD location	Tw (washout)	Wn (filter)	K (control gain)	T1 (phase shift)	T2 (phase shift)	$Lim_{\_P\_POD}$ (limiter)
4153	10	4.21	-2041	0.2083	0.2709	0.5693
7422	10	3.96	8000	0.2255	0.2830	0.9601

Table 11. Parameters of local PODs with active power modulation

POD location	Tw (washout)	Wn (filter)	K (control gain)	T1 (phase shift)	T2 (phase shift)	$Lim_{\_P\_POD}$ (limiter)
4153	10	4.21	196	0.2375	0.2375	0.1
8077	10	3.96	-308	0.2526	0.2526	0.1

Table 12. Parameters of local PODs with reactive power modulation

POD location	Tw (washout)	Wn (filter)	K (control gain)	T1 (phase shift)	T2 (phase shift)	$Lim_{\_P\_POD}$ (limiter)
4153	10	4.21	4290	0.1823	0.3096	0.5693
8077	10	3.96	8100	0.1819	0.3509	1.0000

Wide-Area POD Control Design through Synchronous Generator

To ensure the oscillations can still be damped even when renewables are out of service, wide-area POD through synchronous generators are also developed as the backup of PODs through IBRs. Based on the optimal actuator selection results, the WADC parameters for synchronous generators G4030 and G7208 are listed in Table 13.

Local IBR and Wide-Area POD Control Performance Comparison

To validate the POD damping performance on both Mode 1 and Mode 2, an event in Area 4 (three-phase temporary fault at Line 4040-4079) which can excite Mode 1 and an event in Area 8 (three-phase temporary fault at Line 8030-8158) which can excite both Mode 1 and 2 are simulated with different types of PODs.

Wide-Area POD Control Performance Comparison between Active and Reactive Power Modulation of IBR

Figure 7 (a) and (b) show the bus frequency in Zone 4 without and with wide-area IBR POD control under the two different events. Both Mode 1 and Mode 2 can be damped through wide-area IBR POD control with active and reactive power modulation. The detailed Prony analysis results are listed in Table 14. Compared with Q modulation, P modulation is more effective to support the system recovery to the steady state. Wide-area IBR POD control output with P and Q modulation under the event in Area 4 is shown in Figure 8.

Table 13. Parameters of Wide Area POD through Synchronous Generator

POD location	Tw (washout)	Wn (filter)	K (control gain)	T1 (phase shift)	T2 (phase shift)	$Lim_{\_P\_POD}$ (limiter)
4030	10	4.21	-30	0.4114	0.1371	0.1
7208	10	3.96	-546	0.1178	0.5418	0.1

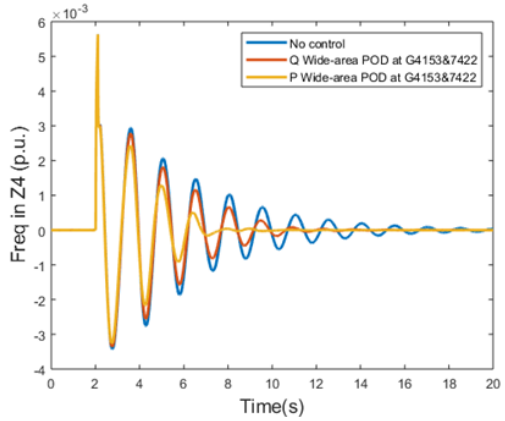

(a) Temporary fault at Line 4040-4079

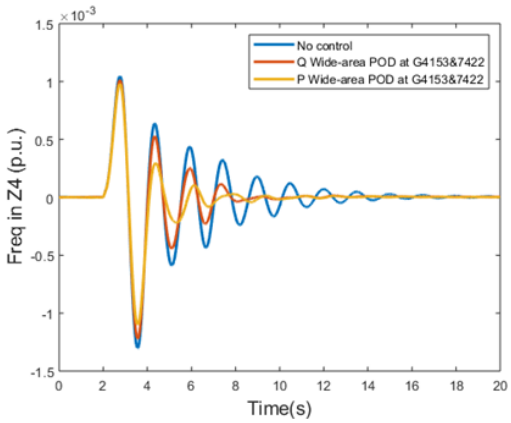

(b) Temporary fault at Line 8030-8158

Figure 7. Wide-area IBR POD control performance comparison between P and Q modulation

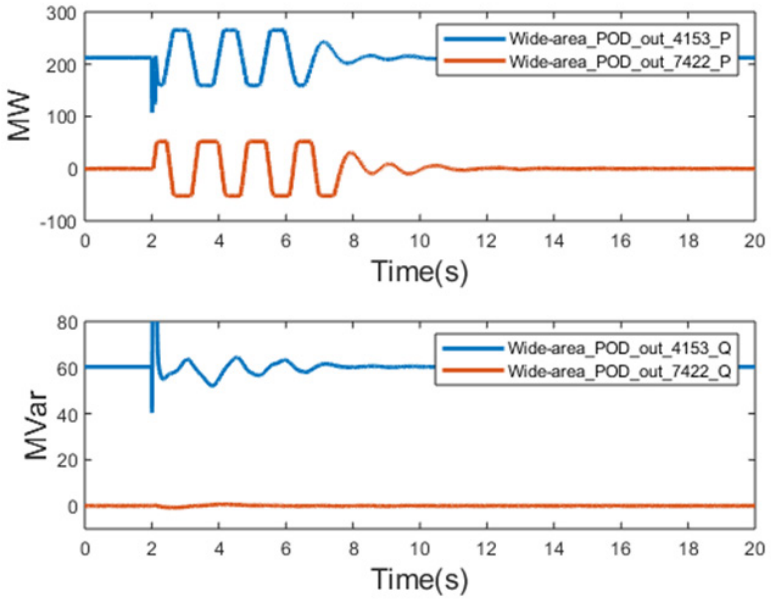

(a) P & Q output of IBR with wide-area POD via P modulation

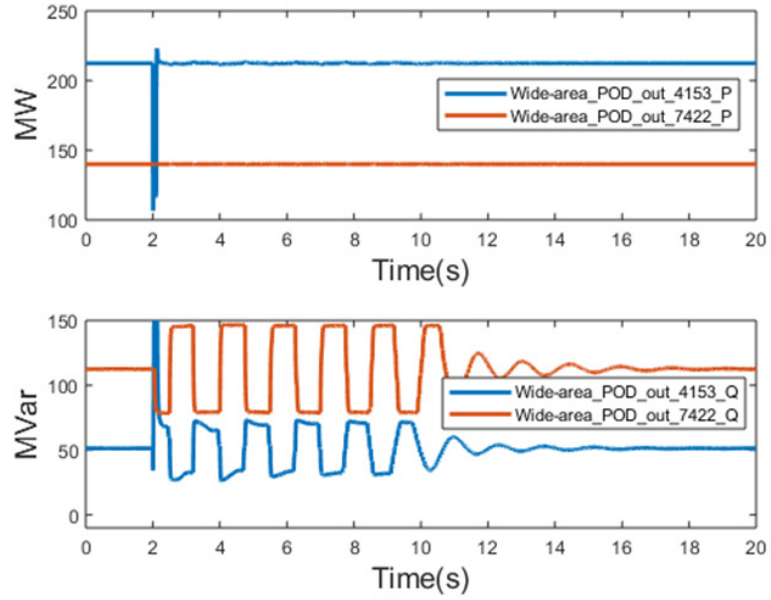

(b) P& Q output of IBR with wide-area POD via Q modulation

Figure 8. Wide-area IBR POD control output through P and Q modulation under event in Zone 4

Local IBR POD Control Performance Comparison between Active and Reactive Power Modulation

Figure 9 (a) and (b) show the bus frequency in Zone 4 without and with local IBR POD control under the two different events. From this figure, both Mode 1 and Mode 2 can be damped through local IBR POD control with active and reactive power modulation. The detailed Prony analysis results are listed in Table 14. Compared with Q modulation, P modulation is more effective to support the system recovery to the steady state. Local IBR POD control output with P and Q modulation under the event in Area 4 is shown in Figure 10.

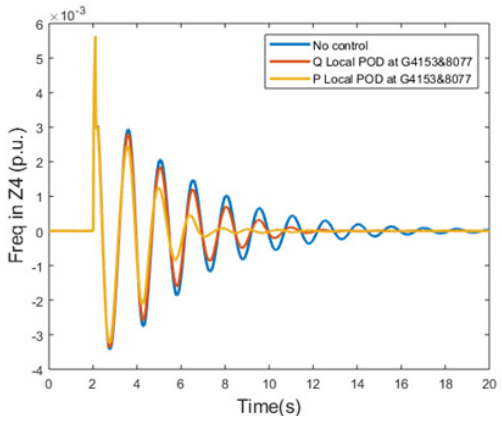

(a) Temporary fault at Line 4040-4079

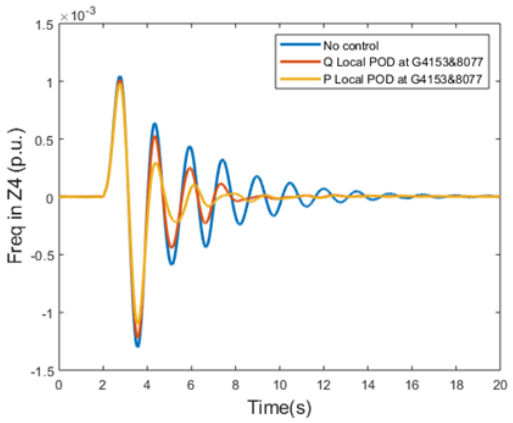

(b) Temporary fault at Line 8030-8158

Figure 9. Local IBR POD control performance comparison between P and Q modulation

Wide-Area and Local POD Control Performance Comparison through Active Power Modulation of IBR

Figure 11 (a) and (b) show the bus frequency in Zone 4 with local or wide-area IBR POD control through active power modulation under the two different events. Compared with local feedback signal, wide-area IBR POD control has a slightly better damping performance on Mode 2. Note though that communication delays have not been considered in this work.

Wide-Area and Local POD Control Performance Comparison through Reactive Power Modulation of IBR

Figure 12 (a) and (b) show the bus frequency in Zone 4 with local or wide-area IBR POD control through reactive power modulation under the two different events. Compared with local feedback signal, wide-area IBR POD control has a slightly better damping performance on Mode 2.

Performance Comparison between Wide-Area POD Control through IBR and Synchronous Generator

Figure 13 (a) and (b) show the bus frequency in Zone 4 with POD through synchronous generator and wide-area IBR POD control through active/reactive power modulation under the two different events. Compared with POD through synchronous generator, wide-area IBR POD control through P modulation is more effective than POD through synchronous generator. Wide-area IBR POD control through Q modulation has similar damping performance as POD through synchronous generator. Detailed Prony analysis results can be seen in Table 14.

Performance Comparison between Local IBR POD Control and Wide-Area POD Control through Synchronous Generator

Figure 14 (a) and (b) show the bus frequency in Zone 4 with POD through synchronous generator and wide-area IBR POD control through active/reactive power modulation under the two different events. Compared with POD through synchronous generator, wide-area IBR POD control through P modulation is more effective than POD through synchronous generator. Wide-area IBR POD control through Q modulation has similar damping performance as POD through synchronous generator. Detailed Prony analysis results can be seen in Table 14.

Summary Table of POD Control Performance with Different Types of POD

The POD performance on damping Mode 1 and Mode 2 for all cases is listed in Table 14, including wide-area IBR POD through active/reactive power modulation, local IBR POD through active/reactive power modulation, and wide-area POD at synchronous generators. Compared with POD through synchronous generator, wide-area and local IBR POD control through active power modulation are more effective than wide-area POD through synchronous generators. Wide-area IBR PODs through reactive power modulation has similar damping performance as wide-area PODs at synchronous generators. The PODs at IBRs and synchronous generators can back up with each other to support the system small-signal stability.

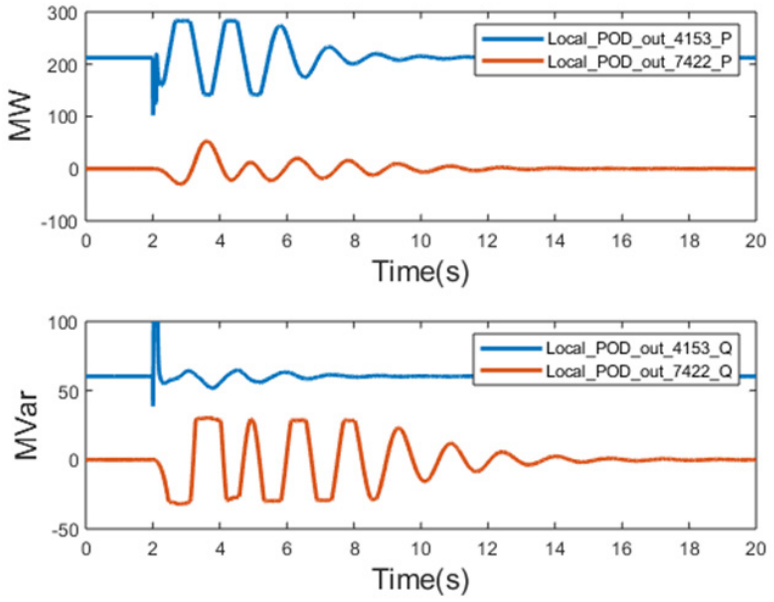

(a) P & Q output of IBR with local POD via P modulation

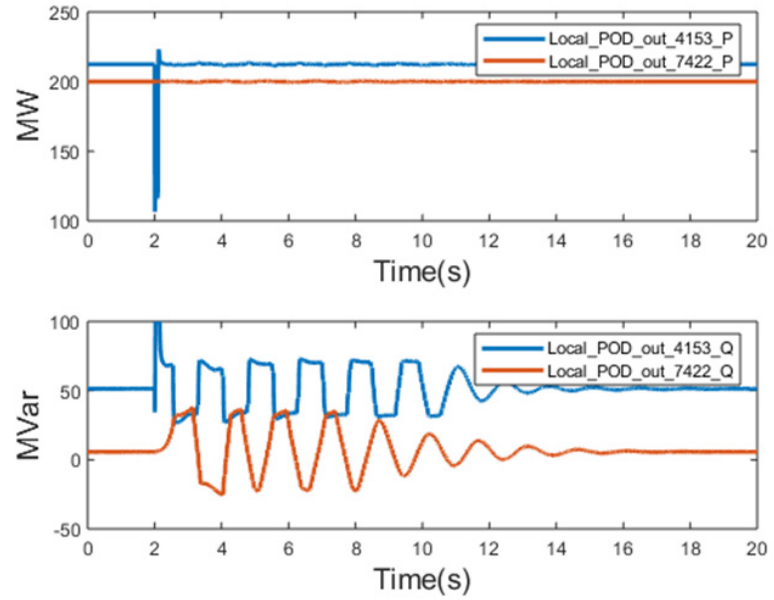

(b) P & Q output of IBR with local POD via Q modulation

Figure 10. Local IBR POD control output through P and Q modulation under event in Zone 4

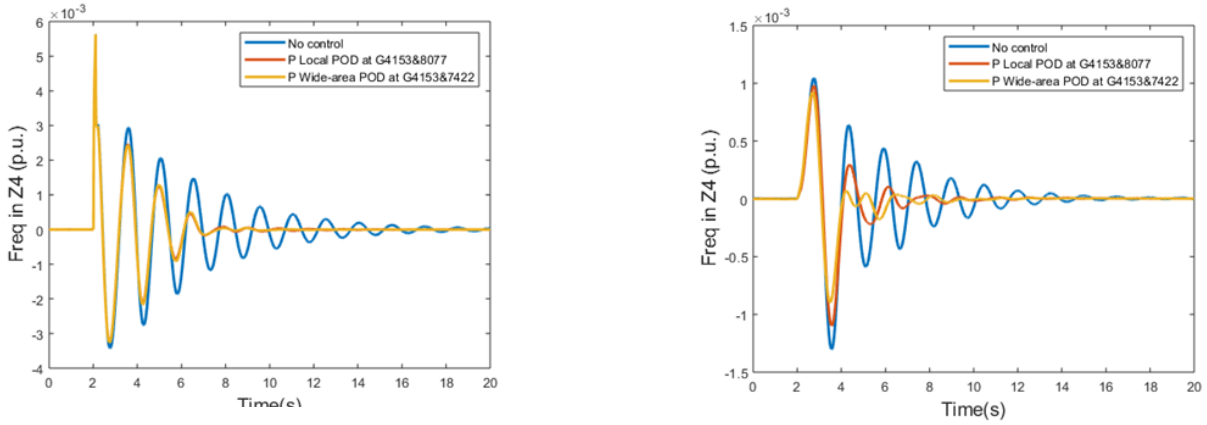

(a) Temporary fault at Line 4040-4079 **(b) Temporary fault at Line 8030-8158**

Figure 11. Wide-area and local IBR POD control performance comparison through active power modulation

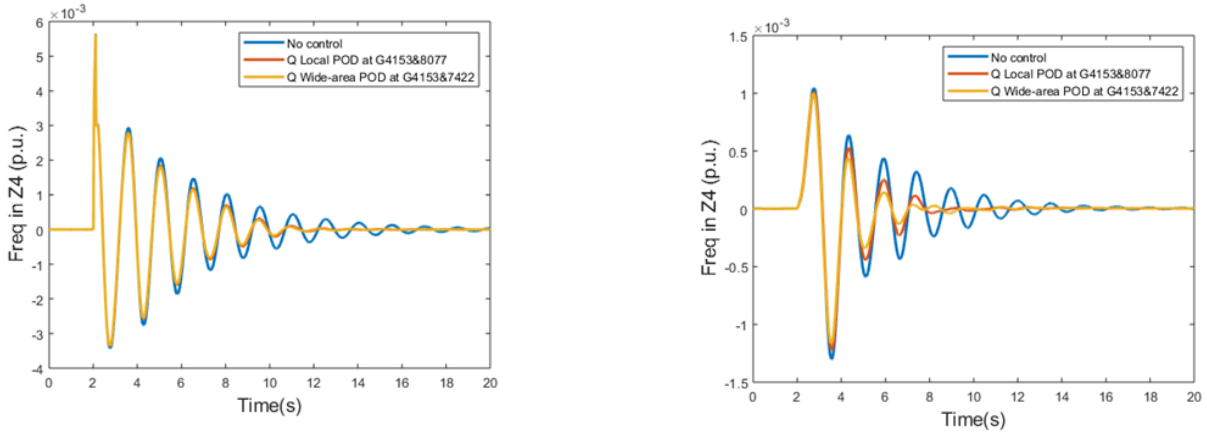

(a) Temporary fault at Line 4040-4079 **(b) Temporary fault at Line 8030-8158**

Figure 12. Wide-area and local IBR POD control performance comparison through reactive power modulation

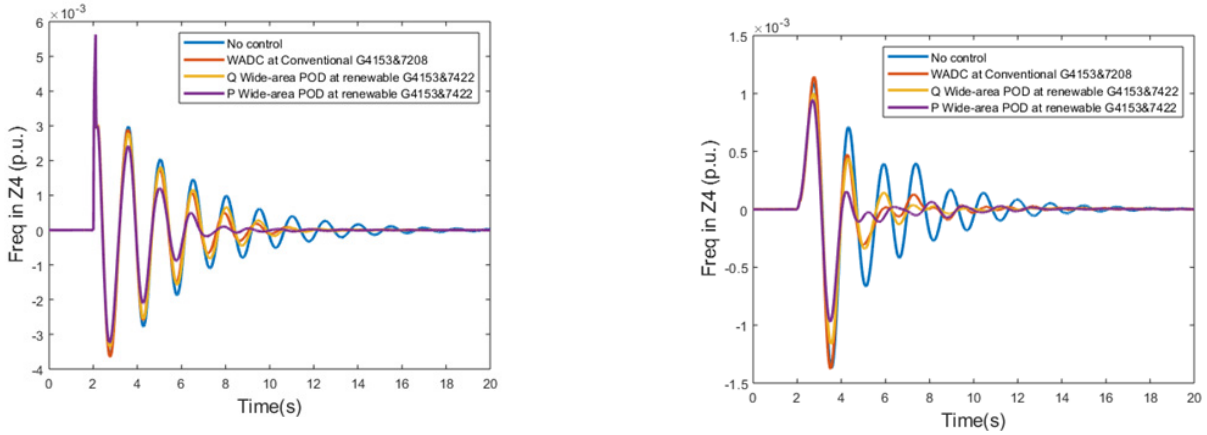

Figure 13. Performance comparison between wide-area POD control through IBR and wide-area POD control through synchronous generator

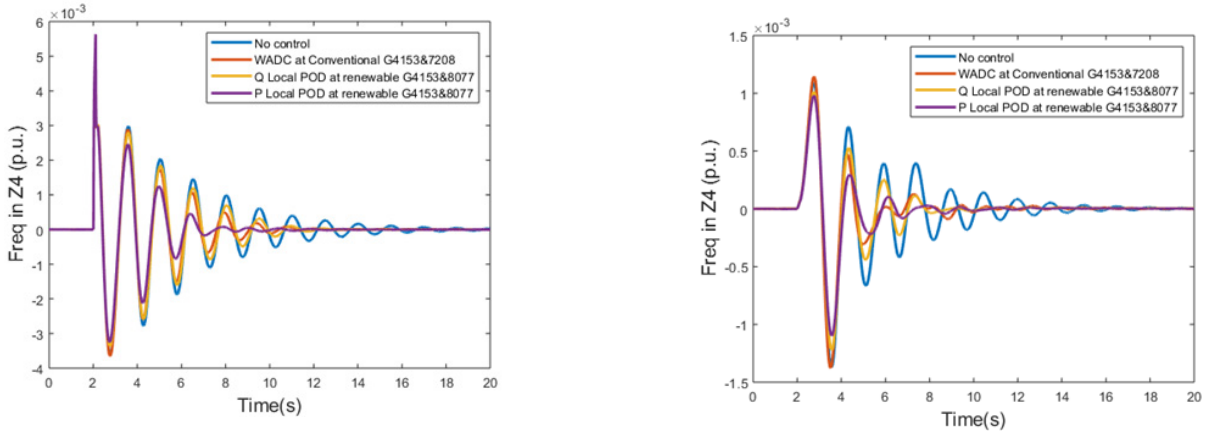

Figure 14. Performance comparison between local POD control through IBR and wide-area POD through synchronous generator

Table 14. Prony analysis results for different types of PODs

POD Type	Actuator	Mode 1		Mode 2	
		Frequency (Hz)	Damping (%)	Frequency (Hz)	Damping (%)
No POD	N/A	0.670	6.22	0.630	8.70
Local POD through P	IBR (4153 & 8077)	0.726	12.71	0.610	>20
Local POD through Q	IBR (4153 & 8077)	0.706	8.00	0.613	15.32
Wide-area POD through P	IBR (4153 & 7422)	0.702	15.00	0.600	>20
Wide-area POD through Q	IBR (4153 & 7422)	0.712	9.64	0.596	17.09
Wide-area POD	Synchronous Generator (4030 & 7208)	0.689	10.36	0.595	18.08

Summary

Wide-area and local POD controllers through IBRs were designed in the synthetic Texas power grid model using a measurement-driven transfer function model. The POD performance was validated to improve the small-signal stability by simulations in PSS/E. A summary of the tasks performed are listed below:

1. Small-signal analysis was conducted to understand the oscillation mode properties in the synthetic Texas power grid. There are two dominant modes (Northeast to South Mode and West to East Mode). These two modes were confirmed by time-domain simulations under different disturbances.
2. The bus frequency difference between Area 4 and Area 7 was selected as the optimal observation signal of the wide-area POD controller. Local POD adopts the local bus frequency signals as its feedback signal.
3. The optimal IBR actuators for the wide-area POD are IBR 4153 in Area 4 and IBR 7422 in Area 7. The optimal synchronous generator actuators for the wide-area POD are generator 4030 in Area 4 and IBR 7208 in Area 7. The optimal IBR actuators for the local POD are IBR 4153 in Area 4 and IBR 8077 in Area 7.
4. The measurement-driven approach was used to design the POD controller with active and reactive power modulation of IBRs. Either active or reactive power modulation of IBRs through wide-area and local POD can suppress the two dominant oscillations effectively.
5. PODs through active power modulation of IBRs are more effective than reactive power modulation of IBRs on suppressing the oscillations. Compared with wide-area PODs, local PODs can get the similar damping performance.
6. Compared to PODs through synchronous generators, PODs through active power modulation of IBRs can damp the oscillations more quickly. PODs through reactive power modulation of IBRs can achieve similar damping performance as PODs through synchronous generators.

References

[1] ACTIVSg2000: 2000-bus synthetic grid on footprint of Texas. https://electricgrids.engr.tamu.edu/electric-grid-test-cases/activsg2000/.

[2] Western Electricity Coordinating Council, "WECC Solar PV Dynamic Model Specification," Salt Lake City, UT, September 2012. Available: https: //www.wecc.biz/Reliability/WECC%20Solar%20 PV%20Dynamic%20Model%20Specification%20-%20September%202012.pdf

[3] J.F. Hauer, C. Demeure, L. Scharf, "Initial results in prony analysis of power system response signals", *IEEE Trans. Power Syst*., vol. 5, no. 1, pp. 80-89, 1990,

[4] M. Tarokh, "Measures for controllability, observability, and fixed modes", *IEEE Trans. Autom. Control,* vol. 37, no. 8, pp. 1268-1273, Aug. 1992.

[5] A. Heniche and I. Kamwa, "Using measures of controllability and observability for input and output selection", *in Proc. 2002 IEEE Int. Conf. Control Applications,* pp. 1248-1251, 2002.

[6] L. P Kunjumuhammed, and B. C. Pal, "Selection of Feedback Signals for Controlling Dynamics in Future Power Transmission Networks", *IEEE Trans. Smart Grid,* vol. 6, no. 3, pp. 1493-1501, May 2015.

[7] A. Heniche, and I. Kamwa, "Control loops selection to damp inter-area oscillations of electrical networks", *IEEE Trans. Power Syst*., vol. 17, no. 2, pp. 378-384, May 2002.

[8] L. Kunjumuhammed, R. Singh, and B. Pal, "Robust signal selection for damping of inter-area oscillations", *IET Gener. Transmiss. Distrib.*, vol. 6, no. 5, pp. 404-416, May 2012.

[9] Ljung L. "System Identification: Theory for the User," *Prentice Hall PTR*, 1999.

[10] M. Aboul-Ela, A. Sallam, J. McCalley, A. Fouad, "Damping controller design for power system oscillations using global signals", *IEEE Trans. Power Syst*., vol. 11, no. 2, pp. 767-773, May 1996.

[11] N. R. Chaudhuri, A. Domahidi, R. Majumder, B. Chaudhuri, P. Korba, S. Ray, and K. Uhlen, "Wide-area power oscillation damping control in Nordic equivalent system", *IET Gener. Transm. Distrib*., vol. 4, no. 10, pp. 1139-1150, Oct. 2010.

[12] J. Zhang, C. Y. Chung, and Y. Han, "A Novel Modal Decomposition Control and Its Application to PSS Design for Damping Inter-area Oscillations in Power Systems," *IEEE Trans. Power Syst.*, vol. 27, no. 4, pp. 2015-2025, Nov. 2012.

[13] A. Magdy, A. Sallam, and J. Mccalley, "Damping controller design for power system oscillations using global signals," *IEEE Trans. Power Syst*., vol. 11, no. 2, pp. 767-773, May 1996.

[14] S.Y. Ruan, G.J. Li, B.T. Obi and Y.Z Sun, "Power system damping from real and reactive power modulations of voltage-source converter station", *IET Gen. Trans. Dist*., vol. 2, no.3, pp. 311-320, June 2008.

NOTE

For further information about EPRI, call the EPRI Customer Assistance Center at 800.313.3774 or e-mail askepri@epri.com.

The Electric Power Research Institute, Inc. (EPRI, www.epri.com) conducts research and development relating to the generation, delivery and use of electricity for the benefit of the public. An independent, nonprofit organization, EPRI brings together its scientists and engineers as well as experts from academia and industry to help address challenges in electricity, including reliability, efficiency, affordability, health, safety and the environment. EPRI also provides technology, policy and economic analyses to drive long-range research and development planning, and supports research in emerging technologies. EPRI members represent 90% of the electricity generated and delivered in the United States with international participation extending to nearly 40 countries. EPRI's principal offices and laboratories are located in Palo Alto, Calif.; Charlotte, N.C.; Knoxville, Tenn.; Dallas, Texas; Lenox, Mass.; and Washington, D.C.

Together . . . Shaping the Future of Energy™

Contact Information

For more information contact the EPRI Customer Assistance Center at 800.313.3774 (askepri@epri.com).

EPRI Resources

Evangelos Farantatos, *Sr. Project Manager*
650.855.2214, efarantatos@epri.com

Deepak Ramasubramanian, *Technical Leader*
865.218.8178, dramasubramanian@epri.com

Lin Zhu, *Technical Leader*
865.218.8058, lzhu@epri.com

Transmission Operations & Bulk System Renewables and Distributed Energy Resources Integration

3002021369 December 2021

EPRI
3420 Hillview Avenue, Palo Alto, California 94304-1338 • PO Box 10412, Palo Alto, California 94303-0813 USA
800.313.3774 • 650.855.2121 • askepri@epri.com • www.epri.com